Synthesis, Structural, Thermal Studies And Biological Activity Of Schiff Base Transition Metal Complexes

Amrish Soam[1*], Gaurav Kumar[2], Nancy[3], Sanjeev Kumar Bhatt[4], Baleshwar Prasad Yadav[5], Bhopal Singh[6]

[1*]Research Scholar, Department of Chemistry, Meerut College, Meerut, Chaudhary Charan Singh University, Meerut Utter Pradesh (amrishsoam93@gmail.com)
[5]Professor, Department of Chemistry, Meerut College, Meerut, Utter Pradesh
[2,3,4]Research Scholar, Department of Chemistry, Meerut College, Meerut, Utter Pradesh
[6]Assistant Professor, Department of Chemistry, Meerut College, Meerut, Utter Pradesh

***Corresponding Author: -** Amrish Soam
Email: amrishsoam93@gmail.com

Abstract
In order to obtain the Schiff base (1-(4-hydroxy-6-methylpyrimidino)-3-phenylthiocarbamide) ligand yields, guanidine and acetoacetic ester interacted. The ligand and its metal complexes are described using thermodynamic investigations (TG and DTA), 1H-NMR, 13C-NMR, UV, and FTIR. The IR spectra show that the ligand binds to the metal ions and behaves neutrally. The thermal behavior of these chelates shows that the anions and ligand molecules disintegrate in the second step after the hydrated complexes lose their water molecules of hydration in the first. The produced metal complexes were then put to the test against Salmonella typhi, Escherichia coli, Staphylococcus aureus, Pseudomonas aeruginosa, Listeria monocytogen, and Listeria candida for their antibacterial, antioxidant, and antidiabetic properties. The activity data indicates that the metal complexes are more effective against one or more bacterial species as antioxidants, antidiabetic agents, and antibacterial agents.

Keywords: Schiff base transition metal complexes, synthesis, antioxidant, antidiabetic , antimicrobial

Introduction

The ligand manufacturing procedure was arguably the most important step in the development of metal complexes with unique properties and novel reactivity. Since different investigations may take into account the ligand's electron donor and acceptor properties, structural functional groups, placement within the coordination sphere, and reactivity of coordination compounds (1). Transition metal schiff base complexes are of special interest to inorganic chemists due to their unique spectroscopic, chemical, and structural properties, which are often greatly influenced by the ligand structure. Because of their diverse structural and physical features, coordination complexes containing substituted ketones have been seen to exhibit a wide range of stereochemistry and bonding interactions. The synthesis of unsymmetrical coordination complexes by the interaction of transition metal ions with tetradentate (2) has garnered increasing attention in the last few years. This understanding includes a deeper understanding of metal–ligand complexation, metal binding site placement, and molecular self-assembly. Acquiring knowledge in these fields will make it possible to use coordination complexes to develop novel, improved systems related to bioengineering, catalysis, and supramolecular chemistry (3-5). The synthesis and characterisation of symmetrical tetradentate Schiff base complexes have been extensively studied, but the unsymmetrical Schiff base complexes derived from acetophenone appear to have received less attention (6). There is no literature on the transition metal complexes of the unsymmetrical Schiff base made from acetophenones and carbohydrazide (7). Thus, continuing our interest in Schiff base ligands and their metal chelates, this work addresses the synthesis and characterization of Schiff base ligand and its complexes (8–10). The coordination behavior of the ligand with transition metal ions (Cr(III), Mn(II), Fe(III), Co(II), Ni(II), Cu(II), Cd(II), Zn(II), UO2(II), and Th(IV)) is investigated before by means of infrared, molar conductance, magnetic moment, solid reflectance, and thermal analysis.

Experimental

Materials and reagents

All chemicals used were of the analytical reagent grade (AR), and of highest purity available. They included 2,6-pyridinedicarboxaldehyde (Sigma), 2-aminopyridine (Sigma), Th(IV) chloride tetrahydrate (Sigma) and Cd(II) and Cu(II) chloride (Sigma) and acetate dihydrate (Prolabo); Cr(III), Co(II) and Ni(II) chloride hexahydrates (BDH); uranyl acetate hexahydrate (Sigma) and ferric chloride hexahydrate (Prolabo). Zinc oxide, disodium salt of ethylenediaminetetraacetic acid (EDTA), (Analar), ammonia solution (33% v/v) and ammonium chloride (El-Nasr pharm. Chem. Co., Egypt). Organic solvents used included absolute ethyl alcohol, diethylether, and dimethylformamide (DMF). 2, 2'-Diphenyl-1-picryl hydrazyl (DPPH) (Sigma), 2,2′-azino-bis-3-ethylbenzthiazoline-6-sulphonic acid (ABTS), Nitrophenyl-α-D-

glucopyranoside (SRL Pvt., Ltd), Tris buffer (Merck), α-amylase ex porcine pancreas (SRL Pvt., Ltd), Dimethyl superoxide (DMSO) (Merck), 3,5-dinitrosalicylic acid (DNSA) (SRL Pvt., Ltd), α-glucosidase for biochemistry ex microorganism (SRL Pvt Ltd), Sodium carbonate (CDH) and Acarbose (Bayer India Limited), Sodium diclofenac, Benzophenone, Ascorbic acid, Antibacterial standards erythromycin (Sigma–Aldrich) were purchased. These solvents came from BDH and were spectroscopic pure. We utilized nitric and hydrochloric acids (Merck). Generally, every preparation involved the use of de-ionized water that was collected from all glass equipment.

Instruments

Using an FT-IR type 1650 spectrophotometer, infrared spectra in the wave number range of 4000–200 cm−1 were recorded. The spectra were identified as KBr pellets. The solid reflectance spectra were measured with a Shimadzu 3101 PC spectrophotometer. The 1H NMR spectra were recorded using Bruker 500 MHz FT-NMR apparatus. The deuterated solvent used was dimethylsulphoxide (DMSO), and the spectra were between 0 and 15 ppm. The thermal studies (TG and DTA) were carried out in a dynamic nitrogen atmosphere (20 mLmin−1) at a heating rate of 10 ◦Cmin−1 using Shimadzu TG-60 H and DTA-60 H thermal analyzers.

Synthesis of metal complexes

The metal complexes of the Schiff base, L were formed by adding hot solution (60 ◦C) of the appropriate metal chloride or acetate (1 mmol) in an ethanol–water mixture (1:1, 25 mL) to the hot solution (60 ◦C) of the Schiff bases (0.30 g/L, 1 mmol) in the same solvent (25 mL). After refluxing the mixture for an hour and stirring it, the complexes precipitated. They were collected by filtration, and then cleaned many times using a 1:1 ethanol–water mixture and diethyl ether (11, 12, 41-45).

Determination of the metal content of the chelates

The metal contents were determined complexometrically by titration against standard EDTA solution at a suitable pH value using the suitable indicator.

Thermal analyses

Thermal study was done by using TGA and DTA analysis.

Biological activities

ABTS.+ scavenging assay

The ABTS radical cation scavenging assay is the method used by Shukla et al. (13), to quantify total antioxidant activity. The ABTS radical cation was prepared by adding 2.4 mM potassium persulfate to an ABTS (stable radical) aqueous solution, and allowing it to sit in the dark for 12–16 hours. Before the experiment, the ABTS solution was diluted in ethanol (1:89 v/v), which produced an absorbance of 0.700± 0.02 at 734 nm. Three replicates of 10 µL samples (1 mg/mL of the relevant organic solvents) and ascorbic acid (concentration 0–15 µM) were combined with 1 mL of diluted ABTS solution. After precisely 30 minutes at 30ºC, the reaction mixture's absorbance was measured at 734 nm in comparison to the blank, which was ethanol.

Radical scavenging activity using DPPH method

The E. acuminata extracts were found to have basically the same radical scavenging action as reported by Shukla et al. (14), but with a few slight alterations. Ascorbic acid (25, 50, 100, 150, and 200 µg) and extracts at different concentrations (25, 50, 100, 150, and 200 µL) were placed into test tubes. To bring the volume up to 100 µL, MeOH was added. Three milliliters of a 0.1 mM DPPH methanol solution were placed inside these tubes, and they were shaken briskly. The tubes were permitted to stand at 27 oC for thirty minutes. The absorbance fluctuations of the generated samples were measured at 512 nm. The inhibition percentage, which was utilized to calculate the radical scavenging activity, was calculated using the following formula:

Measurement of radical scavenging activity % =(OD of blank - OD of sample/ OD of blank) × 100.

Antidiabetic activity

Different extract obtained from fruit were allowed to screen for antidiabetic activity by α-Amylase and α-Glucosidase assay.

Inhibition assay of α-amylase

With minor adjustments, the α-amylase enzyme inhibition procedure adhered to Shukla et al.'s methodology (15). Acarbose (AC) was the standard drug for α-amylase. For all enzymes with the exception of α-amylase, the percentage (%) of inhibition was expressed using the half maximum inhibitory concentration (IC50).

$$\%\ \boldsymbol{of\ inhibition} = \frac{\boldsymbol{Absorbance\ of\ control} - (\boldsymbol{absorbance\ of\ extract})}{\boldsymbol{Absorbance\ of\ control}} \times \mathbf{100}$$

Inhibition assay of α-glucosidase

A slightly modified version of the method used by Kaur et al. [16] was used to carry out the α-glucosidase enzyme inhibition process. Acarbose (AC) served as the reference drug in the α-glucosidase inhibition experiment. The absorbance of the released p-nitrophenol was measured at 410 nm. Every experiment was conducted in triplicate, with

the control being a parallel setup devoid of the test medication. For all the enzymes except α-glucosidase, the half maximal inhibitory concentration (IC50) was calculated using the formula above and reflected the percentage (%) of inhibition.

Antimicrobial activity

The disc-diffusion method was used to measure the antibacterial activity. Many bacteria were extracted from the Microbial Type Culture Collection (MTCC) and stored at -80 ºC. Before being used in the bioassay, microorganisms were inoculated on nutrient agar (Microxpress Ltd.) in petri plates to evaluate their purity. Dimethylsulfoxide (DMSO) was used to make standard medications and stock solutions of plant extracts. A 20 ml sample-saturated sterile disk was placed on top of each 70 mm inoculation plate. The separate bacterial strains were spread out over nutrient agar plates, impregnated with different test samples (20 ml/disc), and the agar plate surface was then seeded. This process produced the agar plates. Following that, the plates were placed in a bacteriological incubator and incubated for a day at 37°C. Millimeters (mm) were used to measure the zones of inhibition in order to assess the antibacterial capabilities. It was believed that inhibitory zones between 12 and 18 mm had significant antibacterial activity, while those less than 12 mm were assumed to have little. (2015) Singh and associates [17].

Statistical analysis

Each experiment was run in triplicate, and the results were reported as Mean± SD. The data were statistically analyzed using One-way ANOVA, and Duncan's test was then run. Mean values were considered statistically significant when $p>0.05$.

Results and discussion

Interpretation of Cu complex

All the newly created compounds were stable at room temperature, non-hygroscopic, and had a light color. These substances are surprisingly soluble in solvents like DMSO and DMF, yet insoluble in water and a number of common organic solvents. According to the analytical results, the complexes showed stoichiometry of types ZnLCl2.2H2O and ML2Cl2 [M = Cu (II)], where L = Schiff base ligand. The compounds' solutions are not electrolytic since their molar conductance values are lower than those predicted for an electrolyte (18).

The IR spectrum of the free ligand was compared with the spectra of metal complexes, which revealed distinctive frequencies of the expected functional groups, in order to investigate the binding mode of the Schiff base to the metal in the complexes. The m(NH) stretch of the CONH group is responsible for the large medium band seen in the IR spectra of the free Schiff's base ligand at 3419 cm-1 (19). Each compound exhibits a minor shift in this band to the side with a higher wave number, suggesting that bonding is not taking place at the CONH group's 'N' location. The carbonyl group m(CO) produces a discernible band in the free ligand at a wavelength of 1634 cm1. In every compound, this band shifted to the side with a lower wave number, suggesting that the carbonyl oxygen participated in the bonding with the metal ions (20). It was discovered that the m(CN) stretch of the azomethine group was the source of a moderate to strong intensity band at 1593 cm_1 in the free ligand (21). It is anticipated that a decrease in the m(CN) absorption frequency and an electron density decrease in the azomethine link will result from the coordination of Schiff's base to the metal ions through the nitrogen atom. The azomethine nitrogen was coordinating with metal ions when this band migrated to the side with a lower wave number in each combination. The m (N-C) stretching vibration of the hydrazine residue is responsible for the medium intensity band at 974 cm-1 (22). This band in the complexes' minor shift to the side with a higher wave number indicates that one nitrogen atom in -N-C-N-is involved in bonding with the metal ions. The [Cu(C24H22O2N8S2)Cl2] complex has a coordinated water molecule, as shown by thermal analysis, which also shows the appearance of a broad band at 3444 cm-1 due to O-H stretching vibration. There have been numerous reports of the furan ring's m(C-O-C) stretching vibrations in the 1020–1250 cm-1 range (23). The oxygen atom in the furan ring is not involved in the bonding process with metal ions, according to the current study's m(C-O-C) stretch, which is shown at 1077 cm-1 and stays constant in the metal complexes (24). The new weak non-ligand bands seen in the complexes' spectra are identified by the frequencies of the m(M-O) and m(M-N) stretching vibrations, respectively. These bands lie in the ranges of 378–410 cm-1 and 468–482 cm-1 (25). The ligand's (Fig. 1) and its Cu (II) complex's 1H NMR spectra were captured in DMSO-d6. The signals at d (11.82) (s, 1H) and d (8.50) (s, 1H) in the free ligand are ascribed to the protons of the (-CONH-) and (-CHN) groups, respectively. The signals of the Cu (II) complex traveled downfield in the regions of d (8.60) (s, 1H) and d (11.93) (s, 1H), demonstrating how the azomethine nitrogen and oxygen atom coordinated their bonding with the metal ions. The aromatic protons of the compound moved downfield at d (7.56-8.48) (m, 7H). The protons of three -CH3 groups are responsible for the signals at d (2.490) (s, 3H, -CH3), d (2.494) (s, 3H, -CH3), and d (2.480) (s, 3H, -CH3).

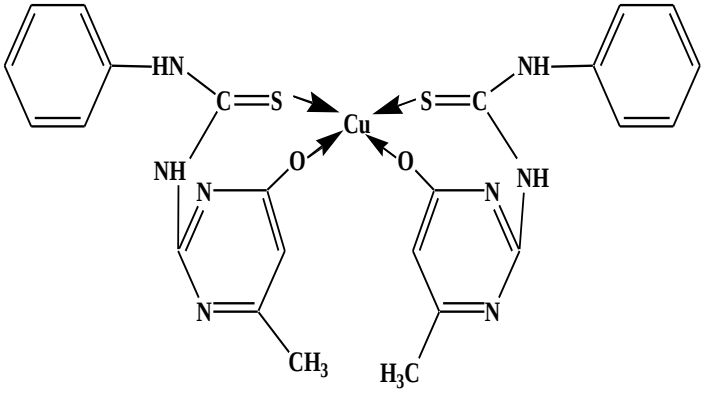

Fig. 1 Cu metal complex of Schiff Base Ligand

Interpretation Ni metal Complex

The newly synthesized materials were stable at room temperature, non-hygroscopic, and light in color. Complexes have remarkable solubility in solvents such as DMSO and DMF, but they remain insoluble in water and a range of common organic solvents.

The IR spectra of the free ligand and the spectra of metal complexes were compared in order to examine the binding mechanism of the Schiff base to the metal in the complexes. This revealed distinctive frequencies of the anticipated functional groups (16). The m(NH) stretch of the CONH group is responsible for the big medium band seen in the IR spectra of the unbound Schiff's base ligand at 3427 cm-1. Each compound exhibits a minor shift in this band to the side with a higher wave number, suggesting that bonding is not taking place at the CONH group's 'N' location. A prominent band in the free ligand is ascribed to the carbonyl group m(CO) at a wavelength of 1647 cm-1. In every compound, this band shifted to the side with a lower wave number, suggesting that the carbonyl oxygen participated in the bonding with the metal ions (27). The m(CN) stretch of the azomethine group was discovered to be the source of a moderate to strong intensity band that was seen at 1538 cm_1 in the free ligand. It is anticipated that a decrease in the m(CN) absorption frequency and an electron density decrease in the azomethine link will occur from the coordination of Schiff's base to the metal ions via the nitrogen atom (28). The azomethine nitrogen was coordinating with metal ions when this band migrated to the side with a lower wave number in each combination. The medium intensity band at 975 cm-1 is caused by the hydrazine residue's m (N-C) stretching vibration. This band in the complexes shifting slightly to the side with a higher wave number (29) confirms that one of the nitrogen atoms in the N-C-N is involved in bonding with the metal ions. Additionally, the thermal analysis verifies that the presence of a coordinated water molecule is indicated by a broad band at 3427 cm-1, which is produced by the O-H stretching vibration of the [Ni(C24H22O2N8S2)Cl2] complex. There have been several reports of the m(C-O-C) stretching vibrations of the furan ring in the range of 1008–1253 cm-1. The oxygen atom in the furan ring is not involved in the bonding with metal ions, according to the current study's m(C-O-C) stretch, which is visible at 1089 cm-1 and is constant throughout the metal complexes (30). The new weak non-ligand bands seen in the complexes' spectra are identified by the frequencies of the m(M-O) and m(M-N) stretching vibrations, respectively. Between 468 and 482 cm-1 and between 378 and 410 cm-1, these bands are visible (31). The ligand's (Fig. 2) and its Ni(II) complex 1H NMR spectra were captured in DMSO-d6. The protons of the (-CONH-) and (-CHN) groups are attributed to the signals at d (10.78) (s, 1H) and d (8.04) (s, 1H) in the free ligand, respectively. The signals from the Ni(II) complex traveled downfield in the regions of d (10.11) (s, 1H) and d (8.05) (s, 1H), demonstrating how the azomethine nitrogen and oxygen atom coordinated their bonding with the metal ions. The complex's aromatic protons migrated downfield at d (6.19-8.05) (m, 7H). The signals at d (2.49) (s, 3H, -CH3), d (2.50) (s, 3H, -CH3), and d (2.51) (s, 3H, -CH3) are caused by the protons of three -CH3 groups.

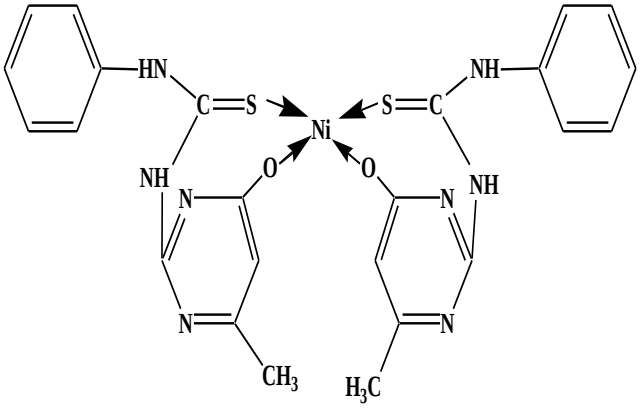

Fig. 2. Ni metal complex of Schiff Base Ligand

Interpretation Zn metal complex

All the newly created compounds were stable at room temperature, non-hygroscopic, and had a light color. These substances are surprisingly soluble in solvents like DMSO and DMF, yet insoluble in water and a number of common organic solvents. The stoichiometry of the complexes were ZnLCl22H2O and ML2Cl2 [M = Zn(II)], where L = Schiff base ligand, respectively. The compounds' solutions are not electrolytic since their molar conductance values are lower than those predicted for an electrolyte.

The IR spectra of the metal complexes and the free ligand were compared in order to investigate the binding mechanism of the Schiff base to the metal in the complexes. The metal complex spectra, which are provided, displayed unique frequencies of the anticipated functional groups (33). The m(NH) stretch of the CONH group is responsible for the large middle band at 3410 cm-1 in the infrared spectra of the free Schiff's base ligand. In all the complexes, this band marginally changes to the higher wave number side, suggesting that the CONH group's 'N' is not bonding (34). A prominent band in the free ligand is ascribed to the carbonyl group m(CO) at a wavelength of 1620 cm-1. In every compound, this band shifted to the side with a lower wave number, suggesting that the carbonyl oxygen participated in the bonding with the metal ions. The m(CN) stretch of the azomethine group was discovered to be the source of a moderate to strong intensity band that was seen at 1583 cm_1 in the free ligand. A decrease in the m(CN) absorption frequency and an increase in the electron density in the azomethine link are predicted as a result of Schiff's base coordination to the metal ions through the nitrogen atom (35). The azomethine nitrogen was coordinating with metal ions when this band migrated to the side with a lower wave number in each combination. Thermal investigation reveals the presence of a coordinated water molecule in the [Zn(C24H22O2N8S2)Cl2] combination with the appearance of a broad band at 3444 cm-1 induced by O-H stretching vibration. There have been several reports of the m(O-C-N) stretching vibrations of the furan ring in the 1020–1250 cm-1 range (30). The oxygen atom in the furan ring is not involved in the bonding with metal ions, according to the current study's m(N-C-O) stretch, which is shown at 1077 cm-1 and stays constant in the metal complexes. The new weak non-ligand bands of the complexes fall into the ranges of 460–492 cm-1 and 370–418 cm-1, respectively, which correspond to the frequencies of the m(M-O) and m(M-N) stretching vibrations (31). The 1H NMR spectra of the Zn (II) complex and the ligand (Fig. 3) in DMSO-d6 were acquired. The protons of the (-CONH-) and (-CHN) groups are attributed to the signals at d (11.82) (s, 1H) and d (8.50) (s, 1H) in the free ligand, respectively. The signals of the Zn (II) complex traveled downfield in the regions of d (8.60) (s, 1H) and d (11.93) (s, 1H), demonstrating how the azomethine nitrogen and oxygen atom coordinated their bonding with the metal ions. The aromatic protons of the compound moved downfield at d (7.56-8.48) (m, 7H). The protons of three -CH3 groups are responsible for the signals at d (2.490) (s, 3H, -CH3), d (2.494) (s, 3H, -CH3), and d (2.480) (s, 3H, -CH3).

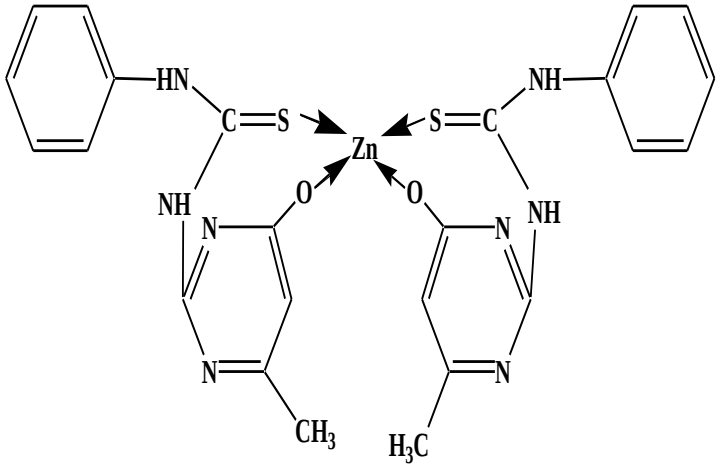

Fig. 3. Zn metal complex of Schiff Base Ligand

Thermal analyses

Two phases of mass losses are visible in the Schiff base complex TG curve across the temperature range of 125 to 600 ◦C. In these phases, mass losses for the first and second stages of breakdown were 100.0% (found 100.0%). It's possible that the C12H17ON4S molecule suffered these mass losses as a result of multiple mass losses that happened within the specified temperature ranges. The Cu(II)-L chelate exhibits three phases of breakdown between 25 and 850 ◦C. Two water molecules are lost during the first two stages of breakdown, which take place between 35 and 430 °C, giving an estimated mass loss of 55.26% (58.25%). An exothermic peak at 150 °C and an endothermic peak at 60 °C accompany these steps in the DTA curve. The elimination of the ligand's organic portion occurs next, at a temperature of 430–850 ◦C, and is expected to result in a mass loss of 20.54% (calculated at 22.15%). At 620 ◦C, the DTA curve displays an endothermic peak. The Zn(II) complex thermogram shows three stages of breakdown, with a temperature range of 35 to 720 ◦C. 2CO2 and C5H9N were lost during the first two phases, resulting in an estimated mass loss of 23.26% (calculated to be 25.48%). An endothermic peak at 55 °C and an exothermic peak at 160 °C were found, which supported this. The C12H17ON4 molecule is removed during the remaining disintegration phases, which occur between 275 and 650 ◦C. An endothermic

peak occurs at 520 ◦C, and the estimated mass loss is 28.36% (calculated to be 30.47%). However, when the organic ligand breaks down and leaves metal oxide as a residue, the Ni(II) complex shows four phases of disintegration with a total mass loss of 85.28% (estimated to be 90.85%), between 28 and 865 ◦C. Three endothermic peaks at 45, 185, and 266 ◦C and one exothermic peak at 505 ◦C support these. Endothermic and exothermic peaks that appear during the entire breakdown process serve as evidence for this.

ABTS method

The total antioxidant activity can be determined using the commonly used ABTS•+ scavenging test. Of all the metal complexes, the Cu complex exhibited the highest ABTS scavenging activity, while the Ni complex displayed the lowest ABTS radical cation scavenging activity. The total antioxidant activity of every sample has been calculated and is shown in Graph 1.

DPPH method

The DPPH radical is a stable organic free radical that has an absorption band at 512 nm. Its absorbance is lost when it takes on an electron or a free radical species, resulting in an apparent visual deterioration from purple to yellow. It has the speed and sensitivity to identify active compounds at low concentrations while handling a large number of samples in a short period of time. The samples' concentration-dependent DPPH scavenging activities are shown in Graph 2. At concentrations between 50 mg/mL and 250 mg/mL, the Cu metal complex exhibited the highest DPPH radical scavenging activity. At dosages up to 200 mg/ml, its ability to scavenge DPPH radicals is comparable to that of the Zn complex, though not substantially so.

Antidiabetic activity

Type-II diabetes mellitus, also known as noninsulin-dependent diabetes mellitus, is a common and serious metabolic condition characterized by abnormally high blood glucose levels (hyperglycaemia) caused by abnormalities in insulin secretion, action, or both (25). Diabetes mellitus (DM) is a chronic and progressive metabolic disorder that affects people of all ages worldwide (26). It is typified by insufficient insulin action, secretion, or both, leading to anomalies in the metabolism of proteins, lipids, and carbohydrates (27). The inability of the pancreas to properly metabolize carbohydrates into energy results in hyperglycemia, or elevated glucose levels in diabetic individuals. This condition causes polyuria, polydipsia, and polyphagia (28). Serious side effects from diabetes hyperglycemia include retinopathy, nephropathy, neuropathy, and organ malfunction. The World Health Organization (WHO) projects that by 2030, diabetes mellitus (DM) would account for the ninth highest cause of mortality among adult patients worldwide, with an estimated 347 million individuals living with the disease (29). A study found that 62.4 million Indians have type 2 diabetes (T2DM) and 77 million have prediabetes (30).

Inhibition assay of α-amylase

The in vitro amylase inhibitory activity of different metals of Schiff base compared with acarbose graphically illustrates the alpha amylase inhibition on varying the concentration of each sample, which helps in the estimation of IC50 values for each sample as well as for standard acarbose. The amount of a metal complex or common drug required to block 50% of an enzyme in a reaction mixture is known as the IC50 value. Every sample shows that amylase activity is inhibited in a dose-dependent manner. A decrease in IC50 levels is associated with increased potency and better therapeutic efficacy. The Ni complex exhibits the best inhibitory action against alpha amylase.

Inhibition assay of α-glucosidase

The graphical representation of glucosidase inhibition in response to varying sample concentrations in Graph 4 facilitates the computation of the IC50 value for each sample in addition to standard acarbose. The in vitro glucosidase inhibitory activity of Schiff base metal complexes in comparison to acarbose is shown in Graph 4. Once more, the combination of Ni and metals exhibited the strongest -glucosidase inhibitory activity. The extremely high potency of Ni complex is demonstrated by the fact that its IC50 value is relatively close to that of acarbose. It has previously been demonstrated that schiff base complexes are potent -glucosidase inhibitors.

Antimicrobial activity

A number of Schiff base metal complexes were tested for their antibacterial activity against two Gram positive (S. aureus, L. monocytogens) and two Gram negative (E. coli, P. aeruginosa) food poisoning bacteria using the disc diffusion method. Results of antibacterial activity of schiff base metal complexes is shown in Table 1. The antibacterial activity of both samples was compared, and the results showed that the Cu complex had the strongest antimicrobial activity against the microorganisms that cause food poisoning.

Conclusion

We used a neutral bidentate Schiff base including donor atoms from carbonyl and azomethine in an experiment. It has been established by numerous spectrum measurements and analytical data that the ligand is bonded to the metal ions. Because of their crucial roles in main group and transition-metal coordination chemistry, as well as the diversity of their structural composition, schiff bases and their metal complexes have been the subject of much research (32). They are

created when primary amines and active carbonyl react with the right solvent. These metal complexes are created by adding the Schiff-base ligand in the proper ratio to a metal precursor under well watched experimental conditions. They have been used by researchers as illuminating chemicals, chelating ligands in coordination chemistry, dyes, initiators of polymerization, and catalysts. Their antibacterial and antifungal effects have been shown in biological tests (33, 34). According to research, there are several ways that copper (Cu) complexes might destroy cancer cells, such as through inducing ROS, damaging DNA, and inhibiting the proteasome (35). However, in recent inorganic synthesis investigations, where researchers have synthesized Cu complexes for a range of medical purposes, Cu-based complexes have come to the forefront. Cu (II) indomethacin complexes, for instance, are used as anti-inflammatory drugs in veterinary medicine (35). Copper is making a comeback since it is found in a lot of naturally occurring biological processes that may regulate copper levels and greatly metabolize it (36).

Schiff-bases are an essential group of substances. In addition to having a high redox potential and being recognized as nano-precursors, a number of metal complexes containing a Schiff-base have been reported, each with a distinct mechanism for stimulating small molecules. A review is conducted on their properties (thermal, magnetic, and electrical) and possible uses in many fields (biology, catalysis, corrosion inhibition, and optical use). Systems of bioinorganic redox enzymes rely heavily on nickel complexes (37–40).

Exothermic and endothermic peaks were confirmed by thermal analysis during the whole breakdown process. In addition to their biological activity, schiff bases and their complexes have a variety of structural characteristics that make them intriguing. Because solvent or water molecules tend to coordinate with zinc ions, it is difficult to form a complex of four coordinated zinc Schiff bases.
This work aims to investigate several Schiff-base compounds based on copper, nickel, and zinc, as these have applications in biology, luminescence, and catalysis.

Table 1- Zone of inhibition (in mm) of bacterial species in Cu, Ni & Zn Complex.

Bacterial species	**Cu Complex 5µg/ml**	**Ni Complex 5µg/ml**	**Zn Complex 5µg/ml**
Escherichia coli	22±0.01	19±0.02	8±0.05
Staphylococcus aureus	13±0.10	15±0.10	11±0.01
Pseudomonas aeruginosa	10±0.06	13±0.06	11±0.02
Listeria monocytogen	22±0.00	20±0.00	8±0.20
Salmonella typhi	19±0.01	21±0.01	11±0.12
Listeria candida	15±0.02	19±0.02	12±0.05

Graph 1- ABTS scavenging activity of isolated compounds of Schiff base metal complexes

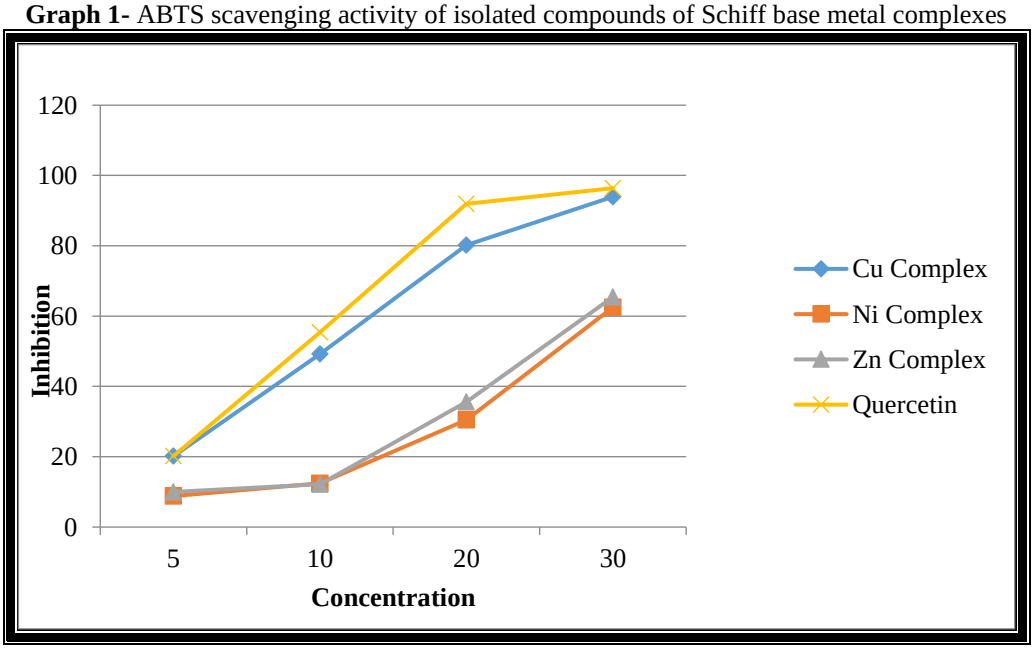

Graph 2- DPPH scavenging activity of isolated compounds of Schiff base metal complexes

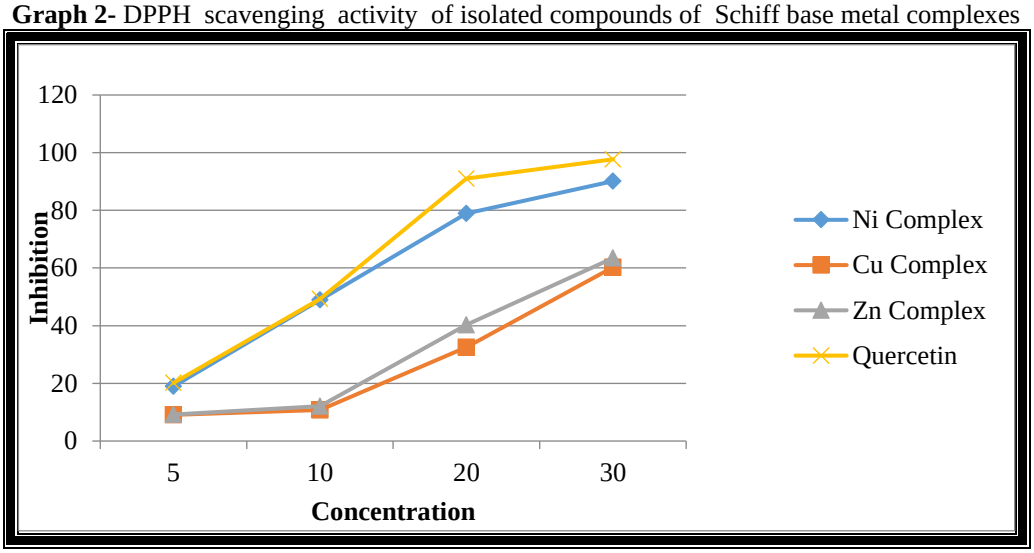

Graph 3- α-Amylase antidiabetic activity of isolated compounds of Schiff base metal complexes.

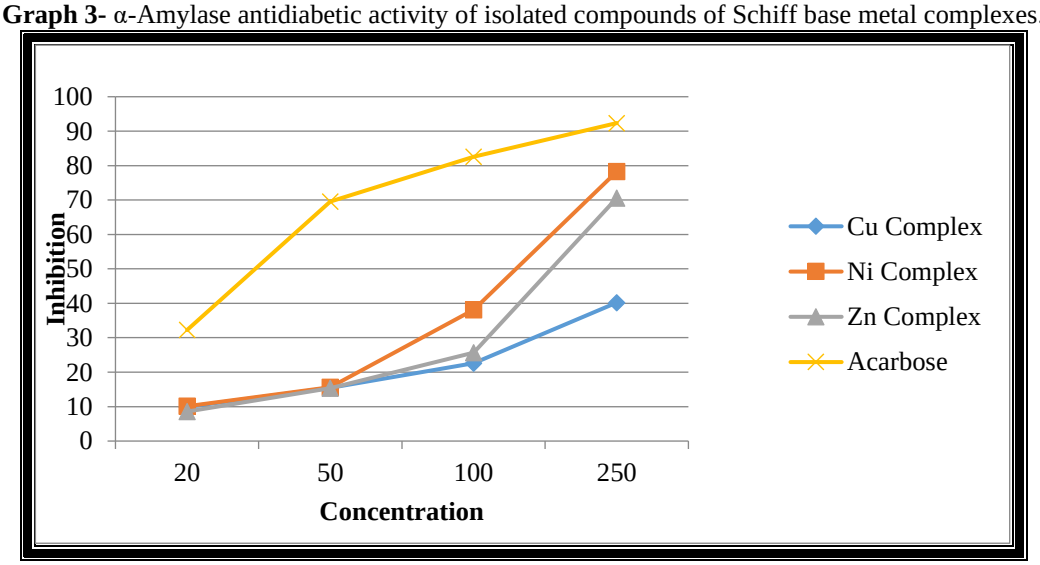

Graph 4- α-Glucosidase antidiabetic activity of isolated compounds of Schiff base metal complexes

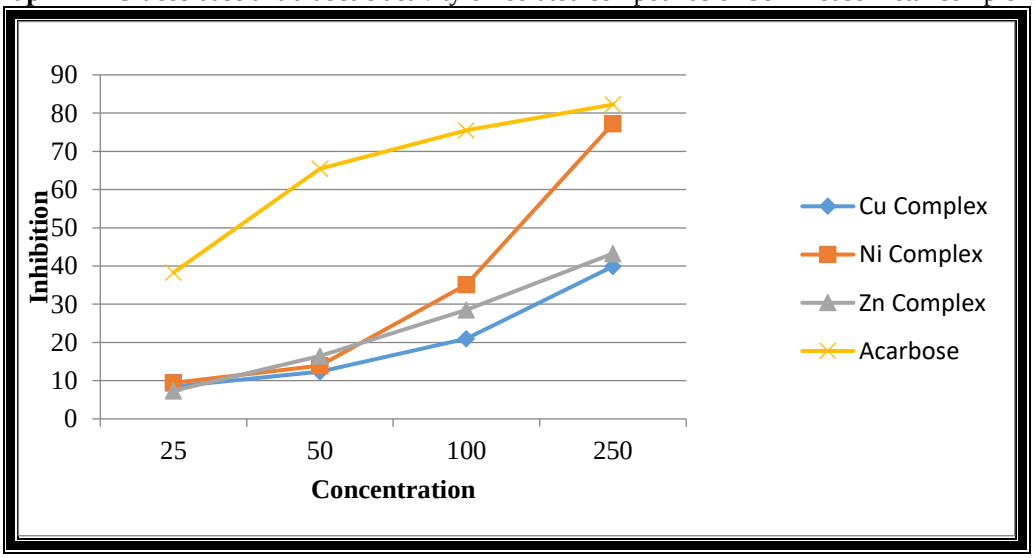

Reference

1. Jain S; Rana M; Sultana M; Mehandi R; Rahisuddin (2022) Schiff Base metal complexes as antimicrobial and anticancer agents, Polycyclic Aromatic Compounds, 5,1-56. DOI: 10.1080/10406638.2022.2117210

2. Jain A; De S; Barman P (2022) Microwave-assisted synthesis and notable applications of Schiff-base and metal complexes: A comparative study, Research on Chemical Intermediates, 48(5),2199-2251. DOI: 10.1007/s11164-022-04708-7
3. Ghobakhloo F; Azarifar D; Mohammadi M; Keypour H; Zeynali H (2022) Copper (II) schiff-base complex modified UiO-66-NH2 (Zr) metal–organic framework catalysts for Knoevenagel condensation–Michael addition–Cyclization reactions, Inorganic Chemistry, 61(12),4825-4841. DOI: 10.1021/acs.inorgchem.1c03284
4. Paul A; Silva T.A; Soliman M.M; Karačić J; Šljukić B; Alegria E.C;, et al. (2022) Benzimidazole Schiff base copper (II) complexes as catalysts for environmental and energy applications: VOC oxidation, oxygen reduction and water splitting reactions, International Journal of Hydrogen Energy, 47(55),23175-23190. DOI: 10.1016/j.ijhydene. 2022.04.271
5. Verma C; Quraishi M.A; Alfantazi A; Rhee K.Y (2021) Corrosion inhibition potential of chitosan based Schiff bases: Design, performance and applications, International Journal of Biological Macromolecules, 184,135-143. DOI: 10.1016/j.ijbiomac.2021.06.049
6. Yadav M; Sharma S; Devi J (2021) Designing, spectroscopic characterization, biological screening and antioxidant activity of mononuclear transition metal complexes of bidentate Schiff base hydrazones, Journal of Chemical Sciences, 133(1):1-22. DOI: 10.1007/s12039-020-01854-6
7. Singh A, Gogoi H.P, Barman P, Guha A.K (2022) Novel thioether Schiff base transition metal complexes: Design, synthesis, characterization, molecular docking, computational, biological and catalytic studies, Applied Organometallic Chemistry, 36:66-73. DOI: 10.1002/aoc.6673
8. Dhingra N; Singh J.B; Singh H.L (2022) Synthesis, spectroscopy, and density functional theory of organotin and organosilicon complexes of bioactive ligands containing nitrogen, sulfur donor atoms as antimicrobial agents: In vitro and in silico studies, Dalton Transactions, 51:8821-8831. DOI: 10.1039/D2DT01051H
9. Abd El-Hamid S.M; Sadeek S.A; El-Farargy A.F; Abd El-Lattif N.S (2021) Synthesis, structural characterization and nematicidal studies of some new N2O2 Schiff base metal complexes, Bulletin of the Chemical Society of Ethiopia, 35(2),315-335. DOI: 10.4314/bcse.v35i2.12
10. Alanazi M.A; Arafa W.A; Althobaiti I.O; Altaleb H.A; Bakr R.B; Elkanzi N.A (2022) Green design, synthesis, and molecular docking study of novel Quinoxaline derivatives with insecticidal potential against Aphis craccivora, ACS Omega, 7(31), 27674-27689. DOI: 10.1021/acsomega.2c03332
11. El-Gammal O.A; Mohamed F.S; Rezk G.N; El-Bindary A.A (2021) Synthesis, characterization, catalytic, DNA binding and antibacterial activities of Co (II), Ni (II) and Cu (II) complexes with new Schiff base ligand, Journal of Molecular Liquids, 326:115223. DOI: 10.1016/j.molliq.2020.115223
12. Wei L; Zhang J; Tan W; Wang G; Li Q; Dong F; et al. (2021) Antifungal activity of double Schiff bases of chitosan derivatives bearing active halogeno-benzenes, International Journal of Biological Macromolecules, 179, 292-298. DOI: 10.1016/j.ijbiomac.2021.02.184
13. Shukla A; Kaur A; Shukla R.K; Anchal (2019) A Comparative Study of In Vitro Antioxidant Potential, Photoprotective Screening of Ehretia acuminata R.Br. Leaves, Indian Drugs, 2019,56(9) 30-36.
14. Shukla A; Kaur A; Shukla R.K; Anchal (2019) Comparative Evaluation of Antioxidant capacity, Total flavonoid and Phenolic content of Ehretia acuminata R. Br. Fruit, Research Journal of Pharmacy and Technology, 12(4) 1811-1816.
15. Shukla A; Kaur A; Shukla R.K (2021) Evaluation of different biological activities of leaves of Ehretia acuminata R.Br, Indian Drugs, 58(4) 42-49.
16. Kaur A; Shukla A; Shukla R.K (2021) In vitro antidiabetic and inti-inflammatory activities of Ehretia acuminata R. Br. Bark, Indian journal of natural product and resources, 12(4) 538-5434512.
17. Singh R; Singh SK; Maharia RS; Garg AN (2015) Identification of new phytoconstituents and antimicrobial activity in stem bark of Mangifera indica (L.), Journal of Pharml Biomedicines and Analysis, 105, 150–155.
18. Iraji M; Salehi M; Malekshah R.E; Khaleghian A: Shamsi F (2022) Liposomal formulation of new arsenic schiff base complex as drug delivery agent in the treatment of acute promyelocytic leukemia and quantum chemical and docking calculations, Journal of Drug Delivery Science and Technology, 75:103600. DOI: 10.1016/j.jddst.2022.103600
19. Hamid S.J; Salih T (2022) Design, synthesis, and anti-inflammatory activity of some Coumarin Schiff Base derivatives: In silico and in vitro study, Drug Design, Development and Therapy, 16:2275. DOI: 10.2147/DDDT.S364746
20. Daravath S; Rambabu A; Ganji N; Ramesh G; Lakshmi P.A (2022) Spectroscopic, quantum chemical calculations, antioxidant, anticancer, antimicrobial, DNA binding and photo physical properties of bioactive Cu (II) complexes obtained from trifluoromethoxy aniline Schiff bases, Journal of Molecular Structure, 1249:131601. DOI: 10.1016/j.molstruc.2021.131601
21. Mane V.A; Palande S.V; Swamy D.K (2021) In vitro antimicrobial activity and plant growth activity study of schiff base ligand (e)-2, 4-diromo-6-{[(2-(2-methoxyphenoxy) ethyl] iminomethyl} phenol and their complexes with transition metals, Journal of Advanced Scientific Research, 12(01 Suppl 2):271-282. DOI: 10.55218/ASR.s12021121sup205
22. Kaur P; Singh R; Kaur V; Talwar D (2021) Anthranilic acid Schiff base as a fluorescent probe for the detection of arsenite and selenite: A detailed investigation of analytical parameters and mechanism for interaction, Analytical Sciences, 37(4):553-560. DOI: 10.2116/analsci.20P102
23. Refat M.S; Saad H.A; Gobouri A.A; Alsawat M; Adam A.M; El-Megharbel S.M (2022) Charge transfer complexation between some transition metal ions with azo Schiff base donor as a smart precursor for synthesis of nano oxides: An

adsorption efficiency for treatment of Congo red dye in wastewater, Journal of Molecular Liquids, 345:117140. DOI: 10.1016/j.molliq.2021.117140
24. Saha S.K; Murmu M; Murmu N.C; Banerjee P (2021) Synthesis, characterization and theoretical exploration of pyrene based Schiff base molecules as corrosion inhibitor, Journal of Molecular Structure, 1245:131098. DOI: 10.1016/j.molstruc.2021.131098
25. Satheesh C.E; Sathish Kumar P.N; Kumara P.R;. Karvembu R; Hosamani A; Nethaji M (2019) Half-sandwich Ru (II) complexes containing (N, O) Schiff base ligands: Catalysts for base-free transfer hydrogenation of ketones, Applied Organometallic Chemistry, 2019;33(10):5111. DOI: 10.1002/aoc.5111
26. Song X.-Q; Wang Z.-G; Wang Y: Huang Y-Y; Sun Y.-X; Ouyang Y, Xie C.-Z ; Xu J.-Y (2020) Syntheses, characterization, DNA/HSA binding ability and antitumor activities of a family of isostructural binuclear lanthanide complexes containing hydrazine Schiff base, Journal of Biomolecule Structure and Dynamics, 38:733–743.
27. El-Gammal O.A; Mohamed F.S; Rezk G.N; El-Bindary A.A (2021) Structural characterization and biological activity of a new metal complexes based of Schiff base. Journal of Molecular Liquids, 330:115522.
28. Kafi-Ahmadi L; Marjani A.P (2019) Mononuclear Schiff base complexes derived from 5-azophenylsalicylaldehyde with Co (ii), Ni (ii) ions: Synthesis, characterization, electrochemical study and antibacterial properties. S. Afr. J. Chem.72:101–107.
29. Shaygan S; Pasdar H; Foroughifar N; Davallo M; Motiee F (2018) Cobalt (II) complexes with Schiff base ligands derived from terephthalaldehyde and ortho-substituted anilines: Synthesis, characterization and antibacterial activity, Applied Sciences, 8:385.
30. Al Momani W.M; Taha Z.A; Ajlouni A.M; Shaqra Q.M.A; Al Zouby M (2013) A study of in vitro antibacterial activity of lanthanides complexes with a tetradentate Schiff base ligand, Asian Pacific Journal of Tropical Biomedicine. 3:367–370.
31. Kaczmarek M.T; Zabiszak M; Nowak M; Jastrzab R (2018) Lanthanides: Schiff base complexes, applications in cancer diagnosis, therapy, and antibacterial activity, Coordination Chemistry Review, 370:42–54.
32. Buldurun K; Turan N; Savcı A; Çolak N (2019) Synthesis, structural characterization and biological activities of metal (II) complexes with Schiff bases derived from 5-bromosalicylaldehyde: Ru (II) complexes transfer hydrogenation. Journal of Saudi Chemistry. Society. 23:205–214.
33. Sagar Babu S.V; Krishna Rao K; Ill LeeY (2017) Synthesis, characterization, luminescence and DNA binding properties of Ln (III)-Schiff base family. Journal of Chil Chemical Society, 62:3447–3453.
34. Wang X; Yang Y.-L: Wang P; Li L; Fan R.-Q; Cao W.-W; Yang B; Wang H; Liu J.-Y (2012) High efficiency co-sensitized solar cell based on luminescent lanthanide complexes with pyridine-2,6-dicarboxylic acid ligands, Dalton Trans, 41,10619–10625.
35. Salihovi´c M; Pazalja M; Halilovi´c S.Š; Veljovi´c E; Mahmutovi´c-Dizdarevi´c I.; Roca, S; Novakovi´c I; Trifunovi´c S (2021) Synthesis, characterization, antimicrobial activity and DFT study of some novel Schiff bases, Journal of Molecular Structure. 1241, 130670.
36. Anzini M; Chelini A; Mancini A; Cappelli A; Frosini M; Ricci L; Valoti M; Magistretti J; Castelli L; Giordani A (2010) Synthesis and biological evaluation of amidine, guanidine, and thiourea derivatives of 2-amino (6-trifluoromethoxy) benzothiazole as neuroprotective agents potentially useful in brain diseases, Journal of Medicinal Chemistry. 53:734–744.
37. Kathiresan S; Annaraj J; Bhuvanesh N.S (2017) Cu (II) and Ni (II) Complexes of Anthracene-Affixed Schiff Base: A Conflict between Covalent and Stacking Interactions with DNA Bases, Chemistry Select, 2:5475–5484.
38. Ejidike I.P; Ajibade P.A (2015) Synthesis, characterization, antioxidant, and antibacterial studies of some metal (II) complexes of tetradentate schiff base ligand:(4E)-4-[(2-(E)-[1-(2, 4-dihydroxyphenyl) ethylidene] aminoethyl) imino] pentan-2-one. Bioinorganic Chemistry and Application, 890734.
39. Keshavayya J; Pandurangappa M; Ravi B (2018) Synthesis, characterization and electrochemical investigations of azo dyes derived from 2-Amino-6-ethoxybenzothiazole, Chemistry Data Collection, 17:13–29.
40. Ashashi N.A; Kumar M; Ul Nisa Z: Frontera A; Sahoo S.C; Sheikh H.N (2021) Solvothermal self-assembly of three lanthanide (III)-succinates: Crystal structure, topological analysis and DFT calculations on water channel. J. Mol. Struct. 2021;1245:131094.
41. Tarannum, N., Kumar, D., & Kumar, N. (2022). β-Cyclodextrin-Based Nanocomposite Derivatives: State of the Art in Synthesis, Characterization and Application in Molecular Recognition. ChemistrySelect, 7(22), e202200140,https://doi.org/10.1002/slct.202200140.
42. AS Nitin* 1 , VeenaChaudhary1 , Yeshpal2# , Nancy2 , Gaurav Kumar2 , Amrish .(2022). THE CURRENT TREND OF CONVERTING AGRICULTURAL/SUGARCANE BAGASSES WASTE IN TO BRICK. European chemical bulletin, 11 (10), 557-568, https://doi.org/10.53555/ecb/2022.11.10.61.
43. Chaudhary, V., & Tomar, A. (2023). A CONCEPTUAL REVIEW ON CONTROLLED RELEASE FERTILIZER. International Journal of Agricultural & Statistical Sciences, 19(1).
44. YN Veena Chaudhary; Bio-Polymer Based Slow Release / Control Release Fertilizer (2023). Research Journal of Agricultural Sciences 14 (5), 1234-1240.
45. Chaudhary, V. (2023). The Significance of Agricultural Wastes in The Construction Sector. Journal of Survey in Fisheries Sciences, 4086-4104, https://doi.org/10.53555/sfs.v10i1.1895